Finite Element Simulation and Comparison of Piezoelectric Vibration-Based Energy Harvesters with Advanced Electric Circuits

A. Hegendörfer* **and J. Mergheim†**

* Institute of Applied Mechanics
Friedrich-Alexander-Universität Erlangen-Nürnberg
Erlangen, Germany
e-mail: andi.hegendoerfer@fau.de

† Institute of Applied Mechanics
Friedrich-Alexander-Universität Erlangen-Nürnberg
Erlangen, Germany
e-mail: julia.mergheim@fau.de

Key words: Smart materials, multiphysics simulation, piezoelectric energy harvesting, numerical simulation, finite element method, coupled problem

Abstract: *A system simulation method based on the Finite-Element Method (FEM) is applied to simulate a bimorph piezoelectric vibration-based energy harvester (PVEH) with different electric circuits: The standard circuit, the synchronized switch harvesting on inductor (SSHI) circuit and the synchronized electric charge extraction (SECE) circuit are considered. Moreover, nonlinear elasticity of the piezoelectric material is taken into account and different magnitudes of base excitations are applied. The holistic FEM-based system simulation approach allows the detailed evaluation of the influences of the considered electric circuits on the vibrational behavior of the PVEH. Furthermore, the harvested energy of the different applied electric circuits with respect to the magnitude of base excitation is compared and results from literature regarding the efficiency of electric circuits are confirmed.*

1 INTRODUCTION

A piezoelectric vibration-based energy harvester (PVEH) is composed of an electromechanical structure along with an electric circuit to extract the energy. The objective of such a device is converting otherwise unused mechanical energy to electrical energy to power e.g. wireless sensors. The piezoelectric effect, used as the energy conversion principle, describes the generation of electrical voltage when the piezoelectric material is mechanically deformed and vice versa.

The applied electric circuit significantly influences the energy output of a PVEH. The choice of the electric circuit depends on the electromechanical coupling of the harvesting structure, the excitation signal and the electric load among others. Therefore, numerous electric circuits have been introduced in the literature to improve the performance of PVEHs. The passive standard circuit is the simplest electric circuit and it was reported, that active circuits like the synchronized switch harvesting on inductor (SSHI) circuit and the synchronized electric charge extraction (SECE) circuit can increase the efficiency of a PVEH significantly compared to the standard circuit [1, 2]. The aim of this contribution is to simulate and compare the energy output of a PVEH with the standard circuit, the SSHI circuit and the SECE circuit for different magnitudes of base excitations. Nonlinear elasticity becomes important for large magnitudes of base excitation, thus, it has to be taken into account in the simulations [3]. Because the electric circuit and the electromechanical structure influence each other, an accurate simulation of a PVEH requires accurate modelling of both the electromechanical structure and the electric circuit. Analytical solutions are restricted to relatively simple geometries of the electromechanical structure and simple electrical loads. Equivalent circuit models describe only the electric behavior of PVEHs and important quantities like the stresses in the material

https://doi.org/10.4995/YIC2021.2021.12177

can not be evaluated. Simulations of PVEHs based on the Finite-Element Method (FEM) have been introduced and allow for arbitrarily shaped geometries and for modeling nonlinear material behavior. Recently, the authors presented a simulation method using only the FEM and allowing for nonlinear electromechanical structures and nonlinear electric circuits [4]. The influence of the electric circuit on the electromechanical structure is considered via the vector of external forces and an implicit time integration scheme is used. Because this method allows for efficient simulations of PVEHs considering nonlinearities of both the electric circuit and the structure, this simulation method is applied within this contribution.

2 GOVERNING EQUATIONS OF PIEZOELECTRICITY

Within this contribution index notation in accordance to [5] is applied. A piezoelectric body is characterized by the help of the linear strain tensor S_{ij} and the electric field E_i

$$S_{ij,i} = \frac{1}{2}\left[u_{i,j} + u_{j,i}\right] \text{ and } E_i = -\varphi_{,i} \tag{1}$$

Here, u_i is the mechanical displacement and φ is the electric voltage. The mechanical and the electric equations for a piezoelectric body Ω are given by the balance of linear momentum and Gauss' law considering that piezoelectric materials are insulating

$$T_{ij,i} = \rho \ddot{u}_j \text{ and } D_{i,i} = 0 \tag{2}$$

Here, ρ is the material density, D_i is the dielectric displacement and T_{ij} are the components of the mechancial stress. A constitutive law that specifies the material behavior must be introduced. In [3] nonlinear elasticity was identified as the primary source of nonlinearity and a nonlinear elastic constitutive law for a 1D setting was introduced, which is here extended to 3D

$$T_{ij} = c^E_{ijkl} S_{kl} - e_{kij} E_k + [c_4 S^3_{11} + c_6 S^5_{11}]\delta_{1i}\delta_{1j} \tag{3}$$

$$D_i = e_{ikl} S_{kl} + \varepsilon^S_{ij} E_j \tag{4}$$

Here, c^E_{ijkl} are the components of the elasticity tensor at constant electric field, e_{ikl} is the piezoelectric constant tensor, ε^S_{ij} is the dielectric constant at constant electric field and δ_{ij} is the Kronecker delta. Nonlinear elastic behavior is thus only introduced in 1-direction, which is a reasonable approach since this is the direction of the largest stresses and strains. The piezoelectric problem can be solved with appropriate boundary conditions

$$u_i = \bar{u}_i \text{ on } \partial\Omega_{Du} \quad \varphi = \bar{\varphi} \text{ on } \partial\Omega_{D\varphi} \quad T_{ij} n_j = \bar{t}_i \text{ on } \partial\Omega_{Nu} \quad D_i n_i = -\bar{Q} \text{ on } \partial\Omega_{N\varphi} \tag{5}$$

The prescribed surface traction $\bar{t}_i$ and the free surface charge density $\bar{Q}$ are introduced. The boundary $\partial\Omega$ of Ω consists of subsets that do not overlap, such that $\partial\Omega_D \cup \partial\Omega_N = \partial\Omega$ and $\partial\Omega_D \cap \partial\Omega_N = \emptyset$.

3 DISCRETIZATION OF THE EQUATIONS

A fundamental step of the FEM is to transform the partial differential equations from their strong formulation into their weak formulation. To obtain the weak formulation, equations (3) and (4) are essentially multiplied by test functions η_j and ξ and subsequently, integration by

parts is applied and the boundary conditions are introduced. The weak form results as

$$\underbrace{\int_\Omega \rho\eta_j\ddot{u}_j \; dV}_{\rightarrow \boldsymbol{f}^{dyn,u}} + \underbrace{\int_\Omega \eta_{j,i}T_{ij} \; dV}_{\rightarrow \boldsymbol{f}^{int,u}} - \underbrace{\int_{\partial\Omega_{Nu}} \eta_j\bar{t}_j \; dA}_{\rightarrow \boldsymbol{f}^{ext,u}} = 0 \tag{6}$$

$$\underbrace{\int_\Omega \xi_{,i}D_i \; dV}_{\rightarrow \boldsymbol{f}^{int,\varphi}} + \underbrace{\int_{\partial\Omega_{N\varphi}} \xi\bar{Q} \; dA}_{\rightarrow \boldsymbol{f}^{ext,\varphi}} = 0 \tag{7}$$

The particular integral terms of the weak form result after the FE discretization in the force terms specified under the brackets. Thereby, $\boldsymbol{f}^{dyn,u}$ is the mechanical inertial force, $\boldsymbol{f}^{int,u}$ is the internal mechanical force, $\boldsymbol{f}^{ext,u}$ is the mechanical external force, $\boldsymbol{f}^{int,\varphi}$ is the electric internal force and $\boldsymbol{f}^{ext,\varphi}$ is the electric external force. The FEM subdivides the domain Ω into small discrete elements and approximates the unknown solutions namely the mechanical displacement and the electric voltage elementwise by means of polynomial ansatz functions and nodal degrees of freedom. Thus, two coupled vector-valued equations for the unknown nodal displacements and electric voltage values result as

$$\boldsymbol{f}^{dyn,u} + \boldsymbol{f}^{int,u} - \boldsymbol{f}^{ext,u} = \boldsymbol{0} \tag{8}$$

$$\boldsymbol{f}^{int,\varphi} + \boldsymbol{f}^{ext,\varphi} = \boldsymbol{0} \tag{9}$$

The coupling to an electric circuit is easier if the electric surface current $-\dot{\bar{Q}}$ appears in the equation. Therefore, the time derivative of equation (9) is used for the system simulations. Furthermore, a mechanical damping force $\boldsymbol{f}^{damp,u}$ is introduced. The resulting system of equations thus becomes

$$\boldsymbol{f}^{dyn,u} + \boldsymbol{f}^{damp,u} + \boldsymbol{f}^{int,u} - \boldsymbol{f}^{ext,u} = \boldsymbol{0} \tag{10}$$

$$\dot{\boldsymbol{f}}^{int,\varphi} - \dot{\boldsymbol{f}}^{ext,\varphi} = \boldsymbol{0} \tag{11}$$

By means of $\boldsymbol{f}^{damp,u}$, a Rayleigh-type damping is modelled. For solving equations (10) and (11) the implicit Bossak-Newmark method is applied for direct time integration. In each time step the nonlinear system of equations is iteratively solved with Newton's method.

4 ELECTRIC CIRCUITS

In this contribution, the standard circuit, the SSHI and the SECE circuit are considered as electric circuits for a PVEH. In the following, the different electric circuits are presented along with a bimorph electromechanical structure introduced in [6].

4.1 Standard Circuit

The simplest way of an AC-DC converter is to use a diode bridge and supply the rectified voltage to an energy storage element. Figure 1 presents this standard circuit coupled with a bimorph electromechanical structure along with the typical waveforms of φ_{el} and $\dot{\bar{Q}}_{el}$ under a harmonic excitation. φ_{el} and $\dot{\bar{Q}}_{el}$ are the voltage and current values at the electrode of the electromechanical structure. They are available from the FEM simulation as decribed in section 5. If the absolute value of the piezoelectric voltage $|\varphi_{el}|$ is smaller than the conductive voltage V_C, the electromechanical structure is in open circuit mode and the current flowing out of the electrode $\dot{\bar{Q}}_{el}$ vanishes. The conductive voltage results from the drop voltage of the diodes V_D and the constant voltage V_{DC}. When $|\varphi_{el}|$ reaches V_C the diode bridge conducts and an electric current $\dot{\bar{Q}}_{el}$ charges the battery.

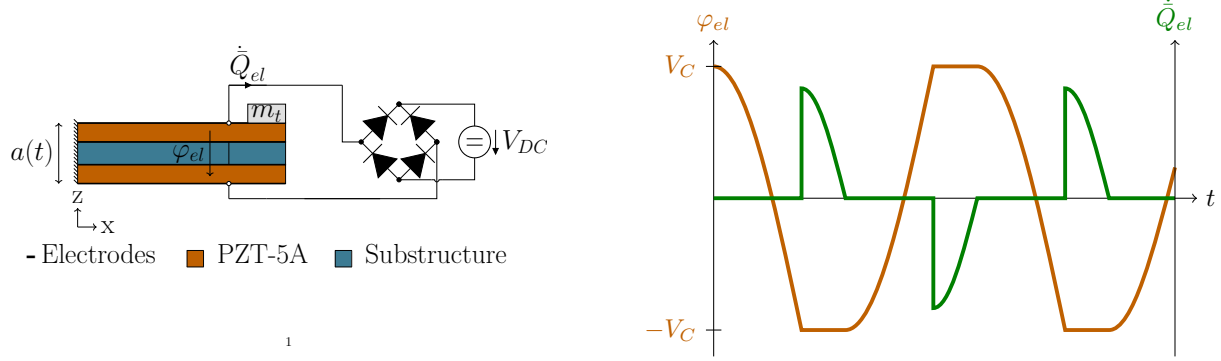

Figure 1: Bimorph electromechanical structure coupled to a standard circuit. The typical waveforms of φ_{el} and $\dot{Q}_{el}$ arising from the standard circuit under a harmonic base excitation of the electromechanical structure are provided.

4.2 SSHI Circuit

The SSHI circuit was introduced in [1] and adds a switch and an inductor (L) to the standard circuit. Figure 2 presents the SSHI circuit coupled to a bimorph electromechanical structure along with the typical waveforms of φ_{el} and $\dot{Q}_{el}$ under harmonic excitation of the structure. When $|\varphi_{el}|$ starts to decrease, the switch is closed, and only the inductor is connected to

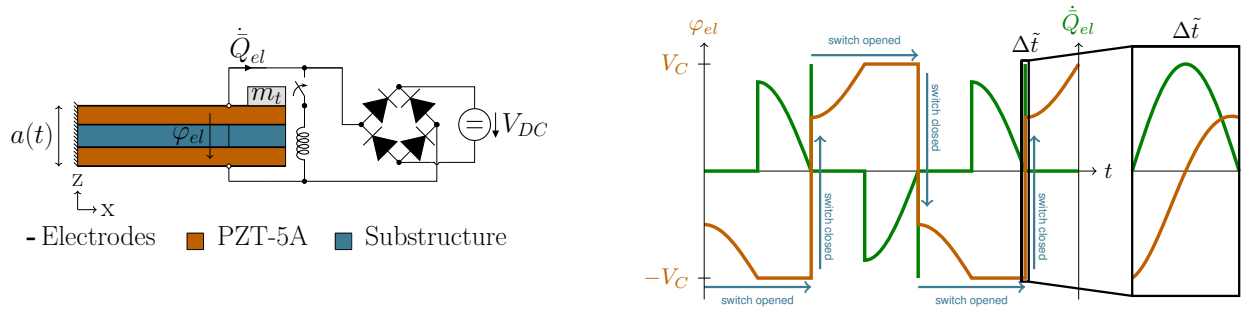

Figure 2: Bimorph electromechanical structure coupled to an SSHI circuit. The typical waveforms of φ_{el} and $\dot{Q}_{el}$ arising from the SSHI circuit under a harmonic base excitation of the electromechanical structure are provided.

the electromechanical structure. Since closing the switch creates an electric resonant circuit consisting of the piezoelectric capacitance and the inductor, the voltage is inverted. When the electric current in the inductor is zero-crossing, the switch is opened again.

4.3 SECE circuit

The SECE circuit was introduced in [2] and consists of a diode rectifier bridge and a buck-boost DCDC converter circuit composed of a switch, an inductor and a diode. To emulate an ideal energy storage device a constant voltage V_{DC} is assumed. During operation of the SECE circuit different phases can be distinguished [7]:

- *Extraction phase.* When the electric voltage φ_{el} reaches its maximum value, the switch is closed and thus only the inductance is connected to the electromechanical structure. Because the piezoelectric capacitance and the inductor form an electric resonance circuit, the electric voltage and the electric current start to oscillate as soon as the switch is closed. When the electric current in the inductance reaches its maximum value, the switch is opened again. When the switch is closed, energy stored in the piezoelectric capacitance is transferred to the inductor. During the extraction phase the absolute value of the

piezoelectric voltage $|\varphi_{el}|$ drops to $\pm 2V_D$. Because the electrical frequencies are usually by orders higher than the mechanical frequencies, the extraction process happens almost instantaneously.

- *Open circuit and freewheeling phase.* The energy stored in the inductor is transferred via the freewheeling diode to the battery. Because the switch is opened, the electromechanical structure is in open circuit mode and the electric current $\dot{\bar{Q}}_{el}$ vanishes.

The inductor is connected either to the electromechanical structure or to the battery, therefore, the electromechanical structure is decoupled from the battery. Figure 3 presents the SECE circuit coupled to a bimorph electromechanical structure along with the typical waveforms of φ_{el}, $\dot{\bar{Q}}_{el}$ and $\dot{Q}_c$ under harmonic excitation of the structure.

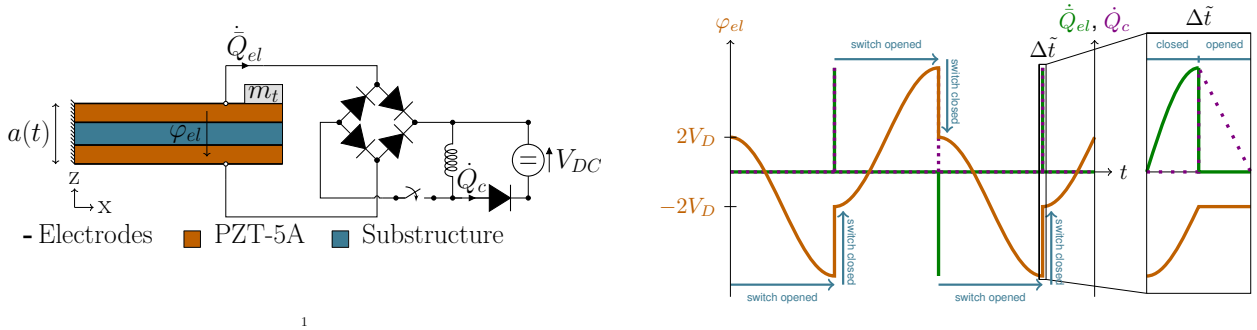

Figure 3: Bimorph electromechanical structure coupled to an SECE circuit. The typical waveforms of φ_{el}, $\dot{\bar{Q}}_{el}$ and $\dot{Q}_c$ arising from the SECE circuit under a harmonic base excitation of the electromechanical structure are provided.

5 FEM SYSTEM SIMULATION

The system simulation method introduced in [4] is applied to simulate a PVEH with a standard, an SSHI and an SECE circuit. Applying the FEM to model an electrode on a surface means to prescribe that all voltage degrees of freedom have the same value φ_{el} on this surface. One reference degree of freedom $\mathcal{F}$ is introduced for the voltage of the electrode. Furthermore, one electrode is assumed to be grounded. Hence, the voltage difference between the electrodes of a PVEH is just the electrical voltage φ_{el} of the non-grounded electrode with the corresponding degree of freedom $\mathcal{F}$. The electric boundary conditions for the grounded electrode is therefore a homogeneous Dirichlet boundary condition with $\bar{\varphi} = 0$. The electric circuit is coupled to the electromechanical structure via the boundary condition of the non-grounded electrode. To account for the influence of the electric circuit on the electromechanical structure, the surface current $\dot{\bar{Q}}_{el}$ leaving the electrode is prescribed. It can be constructed via an inhomogenous Neumann boundary condition

$$\dot{\bar{Q}}_{el} = \int_{\partial\Omega_{Electrode}} \dot{D}_i n_i \, \mathrm{dA} \tag{12}$$

Both, φ_{el} and $\dot{\bar{Q}}_{el}$ correspond to the same reference degree of freedom $\mathcal{F}$ of the non-grounded electrode. The electric current $\dot{\bar{Q}}_{el}$ appears in equation (11) and is introduced in $\dot{\boldsymbol{f}}^{ext,\varphi}$ in the entry for the reference degree of freedom $\mathcal{F}$ as

$$\dot{\boldsymbol{f}}^{ext,\varphi} = \begin{cases} \dot{\bar{Q}}_{el} & \text{for degree of freedom} = \mathcal{F} \\ 0 & \text{for degree of freedom} \neq \mathcal{F} \end{cases} \tag{13}$$

To consider the coupling of various electric circuits with the FE simulation, the relation between the electric current $\dot{\bar{Q}}_{el}$ and the voltage of the non-grounded electrode φ_{el} has to be specified. The implementation of the standard and SSHI circuits are described in detail in [4]. In the following, only the implementation of the SECE circuit is specified.
During operation of the SECE circuit two cases are possible:
Case 1: This is the open circuit case when the switch is opened, and the inductor is not connected to the electromechanical structure. Hence, the electric current $\dot{\bar{Q}}_{el}$ vanishes and thus can be modeled via a homogenous Neumann boundary condition in the FE simulation

$$\dot{\bar{Q}}_{el} = 0 \tag{14}$$

Case 2: In this case the switch is closed, and the inductor is connected to the electromechanical structure. The influence of the inductor on the electromechanical structure is considered via an inhomogeneous Neumann boundary condition. Depending on the sign of φ_{el} the relation is specified as

$$\ddot{\bar{Q}}_{el} = \begin{cases} \frac{\varphi_{el}-2V_D}{L} & \text{if } \varphi_{el} > 0 \\ \frac{\varphi_{el}+2V_D}{L} & \text{if } \varphi_{el} < 0 \end{cases} \tag{15}$$

In figure 4 the logic of the SECE circuit, i.e. the conditions how to switch between cases 1 and 2, is described.

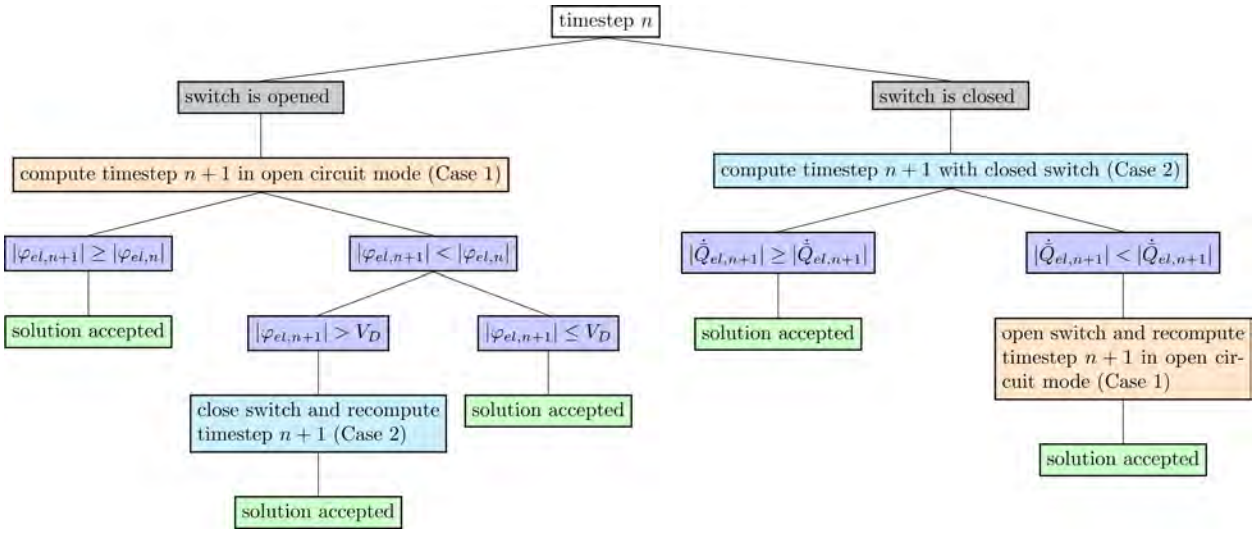

Figure 4: Logic for the definition of boundary conditions for the FE simulation of an electromechanical structure with an SECE circuit.

It has to be prevented in the simulation that the switch is triggered at inappropriate times. After closing the switch, φ_{el} decreases rapidly because the electrical oscillation frequency is usually by orders higher than the mechanical excitation frequency. The rapid decrease of φ_{el} after closing the switch acts like an actuation to the structure, which leads to oscillations of φ_{el} and the electromechanical structure. To prevent that the switch is triggered due to higher order oscillations of φ_{el} caused by its rapid decrease, a time span t_{ns} is introduced during which closing the switch is prohibited. Moreover, φ_{el} flutters during the instationary settling process when the mechanical excitation starts. Therefore, a time span t_{switch} is defined during which closing of the switch is prohibited at the beginning of the simulation.

The harvested energy $\mathcal{E}$ of the SECE circuit can be obtained as

$$\mathcal{E}(t) = \int_0^t V_{DC}\dot{Q}_c \, d\tau \tag{16}$$

whereby $\dot{Q}_c$ depends on the maximum of $\dot{\tilde{Q}}_{el}$ when the switch is opened. In the computation of the harvested energy the dissipation of the diodes is considered, for details please see [7].

6 APPLICATION EXAMPLE

As an application example the bimorph electromechanical structure with a tip mass m_t introduced in [6] coupled to the three different electric circuits is simulated. The bimorph cantilever has a mass mounted on its tip and consists of two layers of PZT-5A bracketing a layer of a passive substructure. The piezoceramic layers are poled in opposite directions. For the substructure, a linear elastic material behavior is assumed and for the PZT-5A the nonlinear piezoelectric constitutive law is applied. Figure 3 presents the considered PVEH and the appendix provides its parameters. A harmonic base acceleration $a(t)$ with a frequency of 47.8 Hz and with three different magnitudes of 0.5, 1 and 9.81 m/s^2 excites the PVEH. The harvested energy and the electric voltage are compared for the standard, the SSHI and the SECE circuit. Some of these results for the standard and SSHI circuits have already been discussed in [4], but here, for the first time, the results for all three circuits are carefully analyzed and compared for different excitation amplitudes.

To prohibit triggering the switch at inappropriate times $t_{ns} = 4$ ms and $t_{switch} = 10.8$ ms are chosen. The bimorph PVEH is discretized with 90 quadratic hexahedral elements. During the extraction phase when the switch is closed the time step size of the Bossak-Newmark time integration scheme is set to 10^{-5} ms since it happens almost instantaneously. After the switch is opened the time step size is set to 10^{-3} ms within a time span $t_{osc} = 2$ ms to precisely capture the higher order oscillation of the electromechanical structure. For the remaining time period a time step size of 10^{-1} ms is used.

Firstly, a magnitude of 0.5 m/s^2 of the harmonic base acceleration is applied. Figure 5 presents the results for φ_{el} and the harvested energy of the standard , the SSHI and the SECE circuit from [4]. The considered time period is 0 to 200 ms. The standard circuit harvests around 0.0014 mJ which is approximately 125% of the energy harvested by the SECE circuit and around 300% of the amount of energy harvested by the SSHI circuit. As shown in figure 5, left, the SSHI circuit rapidly changes the potential when the switch is closed by a much larger amount than the SECE circuit. Therefore, the excitation of high frequency vibration modes is more significant for the SSHI circuit and the energy dissipation is higher than for the SECE circuit. Moreover, the advantage of the SSHI circuit is usually to extend the time during which the diode rectifier is conducting. But in this case, due to the higher order vibration modes, the conduction time is actually shorter than for the standard circuit which can be seen in the zoom-in of the diagram in figure 5, left. Because of the higher dissipation due to the high frequency vibrations and the short conduction time, the SSHI circuit is the least effective here and harvests the least amount of energy. For a base acceleration of 0.5 m/s^2 the passive standard circuit, that does not excite high frequency vibration modes, is more efficient than the SSHI circuit and SECE circuit.

Figure 6 presents the results for φ_{el} and the harvested energy when a magnitude of 1 m/s^2 of harmonic base acceleration is applied. The considered electric circuits harvest nearly the same amount of energy within a time period of 200 ms namely around 0.006-0.007 mJ. The change of φ_{el} caused by the switching events of the SSHI and the SECE circuit are in the same order and therefore approximately an equal amount of energy is dissipated by the high frequency vibration modes. Furthermore, when a magnitude of 1 m/s^2 of harmonic base excitation is applied, the SSHI circuit extends the time fraction during which the diode bridge conducts compared to the standard circuit, as shown in the zoom-in in figure 6, left. The standard circuit does not excite high frequency vibration modes and has the same efficiency for the considered PVEH

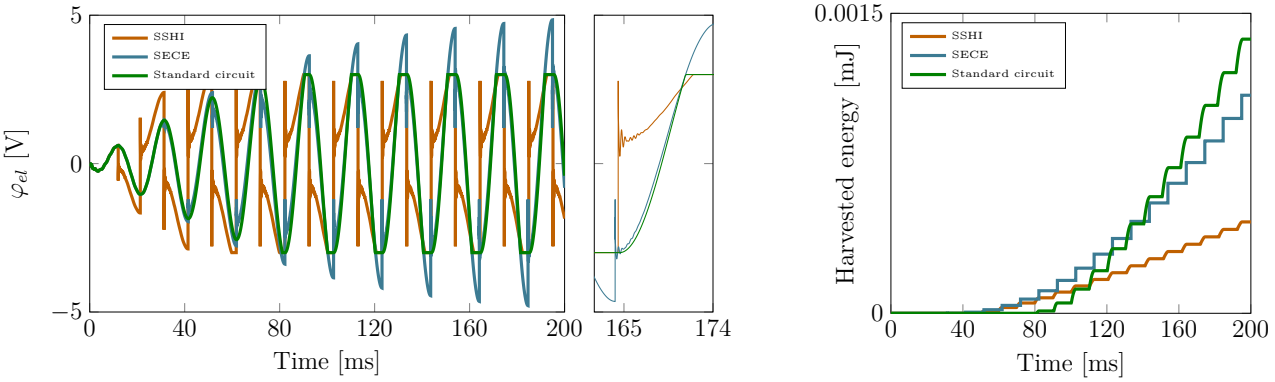

Figure 5: Electrode voltage φ_{el} and harvested energy $\mathcal{E}$ of the bimorph PVEH with standard, SSHI and SECE circuit under a harmonic base acceleration of 0.5 m/s^2 and a frequency of 48.7 Hz.

like the SSHI and SECE circuit for the considered time period. While the standard circuit and the SSHI circuit limit the piezoelectric voltage φ_{el} to $\pm V_C$, the SECE circuit does not limit φ_{el} and therefore the highest values of φ_{el} are reached.

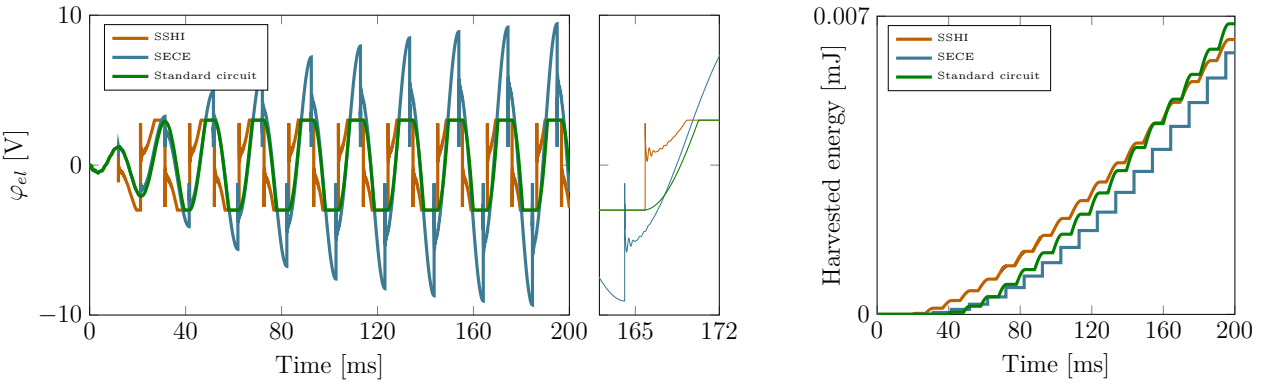

Figure 6: Electrode voltage φ_{el} and harvested energy $\mathcal{E}$ of the bimorph PVEH with standard, SSHI and SECE circuit under a harmonic base acceleration of 1 m/s^2 and a frequency of 48.7 Hz.

Figure 7 presents the results for φ_{el} and the harvested energy for the standard circuit, the SSHI circuit and the SECE circuit when a harmonic base acceleration with a magnitude of 9.81 m/s^2 is applied. The SECE circuit harvests approximately 0.3 mJ during 200 ms, which is around three times the amount of energy harvested by the standard circuit or the SSHI circuit. The high level of applied base acceleration would lead to high open circuit piezoelectric voltages compared to the conductive voltage V_C of the standard circuit and the SSHI circuit, which limit φ_{el} to $\pm V_C$. Therefore, the actuation of the electromechanical structure caused by voltage inversion for the SSHI circuit and, thus, the related dissipation of energy, are relatively small. However, because of the high level of mechanical base acceleration the advantage of the SSHI circuit, namely to extend the conduction time of the diode bridge, does not significantly improve the efficiency compared to the standard circuit, as is shown in the zoom-in in figure 7, left. Therefore, both the standard circuit and SSHI circuit harvest nearly the same amount of energy, namely around 0.09 mJ. In contrast, the harvested energy is independent of the applied electric load when the SECE circuit is used. Therefore, the SECE circuit is more efficient than the standard circuit and the SSHI circuit for this high level of base acceleration. To optimize the harvested energy of the standard circuit and the SSHI circuit for this setting a DC-DC converter must be applied after the diode bridge to regulate the conductive voltage V_C. This flexible adjustment of V_C to the current conditions would allow to harvest significantly more energy with the standard circuit and the SSHI circuit than for a constant conductive voltage

V_C [8].

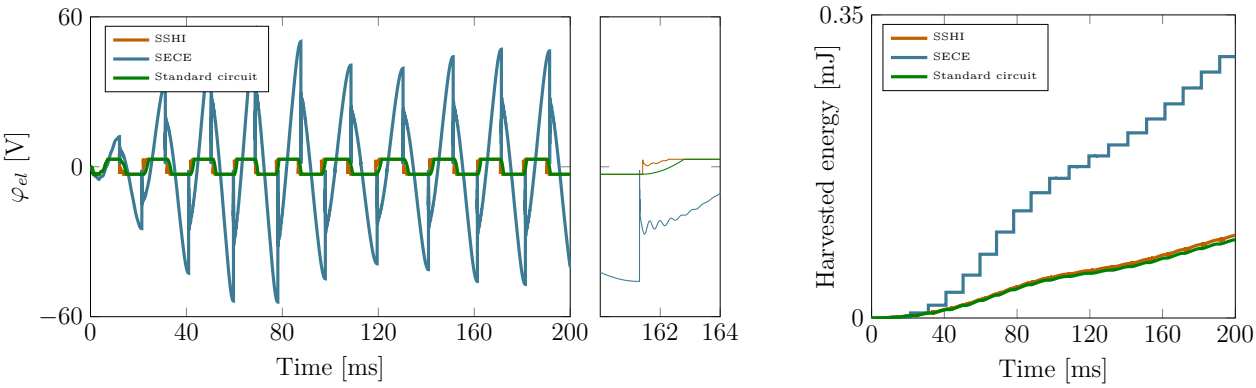

Figure 7: Electrode voltage φ_{el} and harvested energy $\mathcal{E}$ of the bimorph PVEH with standard, SSHI and SECE circuit under a harmonic base acceleration of 9.81 m/s^2 and a frequency of 48.7 Hz.

To sum up the simulation results, the drawback of the SSHI and the SECE circuit compared to the standard circuit is additional dissipation because of higher order vibration modes excited by switching events. This observation is consistent with the literature [9]. Furthermore, the simulation results confirm the advantage of the SECE circuit namely the independence of the harvested energy on the electric load. The efficiency of the standard and the SSHI circuit decreases compared to the SECE circuit for high levels of base acceleration. To improve the efficiency of the standard and the SSHI circuit a flexible adaption of the conductive voltage V_C to the current harvesting conditions would be necessary.

7 CONCLUSION

The FEM based system simulation method introduced in [4] is here applied to simulate a PVEH with three different circuits, a standard, an SSHI and an SECE circuit, and to compare their efficiency. Nonlinear elasticity of the electromechanical structure is taken into account and different magnitudes of a harmonic base acceleration are considered. Consistently with the literature, the SECE circuit and the SSHI circuit dissipate energy compared to the standard circuit through higher order vibration modes caused by switching events. This additional dissipated energy reduces the efficiency of the respective electric circuits. Because the harvested energy is independent of the electric load, the SECE circuit is more efficient than the considered standard circuit and the SSHI circuit without an additional DC voltage regulation stage for high levels of base accelerations. These results demonstrate the applicability of the system simulation method of [4] to develop or improve PVEHs.

ACKNOWLEDGEMENTS

The authors gratefully acknowledge financial support for this work by the Deutsche Forschungsgemeinschaft under GRK2495/C.

REFERENCES

[1] Guyomar D., Badel A., Lefeuvre E., et al. Toward energy harvesting using active materials and conversion improvement by nonlinear processing. *IEEE Transactions of Ultrasonics, Ferroelectrics, and Frequency Control*, Vol. **52**, pp. 584-595, (2005).

[2] Lefeuvre, E., Badel, A., Richard, C., et. al. Piezoelectric Energy Harvesting Device Optimization by Synchronous Electric Charge Extraction. *Journal of Intelligent Material Systems and Structures*, Vol. **16**, pp. 865-876, (2005).

[3] Stanton S.C., Erturk A., Mann B.P., et al. Nonlinear nonconservative behavior and modeling of piezoelectric energy harvesters including proofmass effects. *Journal of Intelligent Material Systems and Structures*, Vol. **23**, pp. 685-704, (2012).

[4] Hegendörfer, A., Steinmann P. and Mergheim, J. Nonlinear finite element system simulation of piezoelectric vibration based energy harvesters. *Journal of Intelligent Material Systems and Structures*, Accepted. DOI 10.1177/1045389X211048222.

[5] Institute of Electrical and Electronics Engineers (IEEE) IEEE standard on piezoelectricity, ANSI-IEEE Std. 176-1987 (1988). Available at: https://ieeexplore.ieee.org/stamp/stamp.jsp?tp=&arnumber=26560 (accessed 02 December 2020).

[6] Erturk A. and Inman D.J. An experimentally validated bimorph cantilever model for piezoelectric energy harvesting from base excitations. *Smart Materials and Structures*, Vol. **18**, 025009, (2009).

[7] Chen, C., Zhao, B. and Liang J. Revisit of synchronized electric charge extraction (SECE) in piezoelectric energy harvesting by using impedance modeling. *Smart Materials and Structures*, Vol. **28**, 105053, (2019).

[8] Ottman G.K., Hofmann H.F., Bhatt A.C., et al. Adaptive piezoelectric energy harvesting circuit for wireless remote power supply. *IEEE Transactions on Power Electronics*, Vol. **17**, pp. 669-676, (2002).

[9] Dorsch P., Bartsch T., Hubert F., et al. Implementation and Validation of a Two-Stage Energy Extraction Circuit for a Self Sustained Asset-Tracking System. *Sensors*, Vol. **19**, 1330, (2019).

APPENDIX

In the following, material parameters for PZT-5A used in this contribution are provided and both the parameters of the bimorph electromechanical structure from [6] and the parameters of the application example (Figure 3) are listed.

Width of the beam [mm]	31.8
Length of the beam [mm]	50.8
E modulus substructure [GPa]	105
Thickness substructure [mm]	0.14
Thickness PZT [mm]	0.26 (each)
Density substructure [kg/m^3]	9000
Tip mass m_t [kg]	0.012
Inductivity [mH]	0.1
V_D [V]	0.6
$V_{DC}[V]$	1.8

$$\boldsymbol{c}^E = \begin{bmatrix} 120.3 & 75.2 & 75.1 & 0 & 0 & 0 \\ 75.2 & 120.3 & 75.1 & 0 & 0 & 0 \\ 75.1 & 75.1 & 110.9 & 0 & 0 & 0 \\ 0 & 0 & 0 & 21.1 & 0 & 0 \\ 0 & 0 & 0 & 0 & 21.1 & 0 \\ 0 & 0 & 0 & 0 & 0 & 22.6 \end{bmatrix} \text{GPa}$$

$$\boldsymbol{e} = \begin{bmatrix} 0 & 0 & 0 & 0 & 12.3 & 0 \\ 0 & 0 & 0 & 12.3 & 0 & 0 \\ -5.4 & -5.4 & 15.8 & 0 & 0 & 0 \end{bmatrix} \frac{\text{C}}{\text{m}^2}$$

$$\boldsymbol{\varepsilon}^S = \begin{bmatrix} 813.7 & 0 & 0 \\ 0 & 813.7 & 0 \\ 0 & 0 & 731.9 \end{bmatrix} \times 10^{-11} \frac{\text{F}}{\text{m}}$$

The nonlinear coefficients in equation (3) for the nonlinear piezoelectric constitutive law were identified in [3] as $c_4 = -9.7727 \times 10^{17}$ Pa and $c_6 = 1.4700 \times 10^{26}$ Pa for the considered PZT-5A material.